

# Non-destructive testing and assembly quality evaluation of IFOG optical path

HAOTING LIU<sup>a,\*</sup>, YUZHOU MA<sup>b</sup>, WEI WANG<sup>c</sup>, BEIBEI YAN<sup>c</sup>

<sup>a</sup>Beijing Engineering Research Center of Industrial Spectrum Imaging, School of Automation and Electrical Engineering, University of Science and Technology Beijing, No. 30 Xueyuan Road, Haidian District, Beijing, China, 100083

<sup>b</sup>Beijing Aerospace Times Optical-electronic Technology Co., Ltd., No. 1 Fengying East Road, Haidian District, Beijing, China, 100094

<sup>c</sup>Beijing Institute of Aerospace Control Device, No. 52 Yongding Road, Haidian District, Beijing, China, 100854

Because many assembly faults, such as the improper layout or the human error-caused problem, cannot be avoided, the optical path of Interferometric Fiber Optic Gyroscope (IFOG) may be damaged. To conquer that problem, the optical path is divided into the front-end optical path, the back-end optical path, and the inner side of fiber optic coil; and three non-destructive testing methods are developed: the laser injection method, the Optical Time Domain Reflectometer (OTDR) method, and the infrared image analysis method. The support vector machine is utilized to assess the assembly quality. Many practical applications have manifested the effectiveness of proposed method.

(Received November 15, 2017, accepted April 8, 2019)

**Keywords:** IFOG Optical path, Non-destructive testing, Assembly quality evaluation

## 1. Introduction

The Interferometric Fiber Optic Gyroscope (IFOG) [1] is a kind of all-solid-state and miniaturized inertia device which can realize the measurement of rotation rate. Fig. 1 shows the structure sketch map of a kind of IFOG. From Fig. 1, an IFOG at least include six parts: the erbium doped light source, the coupler, the integrated optical chip, the fiber-optic coil, the detector, and the digital circuit system. Customarily, the former five parts are called the optical path of IFOG. Comparing with the design of IFOG, the manufacturing and the assembly of it are also not easy tasks. They need to consider a series of factors, such as the materials, the operation procedure, the circuit layout, the application environment, and even the cost, etc. Because the IFOG uses the optoelectronic elements and the fibers to assemble product, the fiber splicing [2] is its basic assembly process.

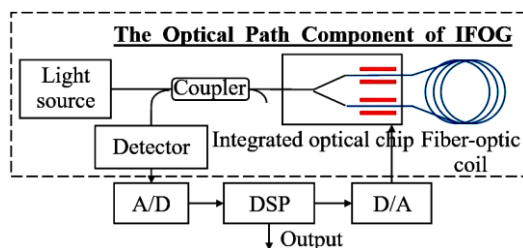


Fig. 1. The working principle diagram of a kind of IFOG

Many problems will happen when assembling IFOG optical path. The first problem is the low quality element-caused unqualified assembly. This problem mainly will be

revealed when the performances of optoelectronic parts and components cannot fulfil the application requirement of user. It can be exposed by the final output measurement of IFOG optical path or a series of environment adaptability experiments [3]. The second problem is the improper layout-caused unqualified assembly. This problem cannot be foresaw or identified easily because it will happen only in some extreme situations. The computer simulation [4] can solve that problem to some extent. The third problem is the human error-caused unqualified assembly [5]. Currently, the manufacturing and the assembly of IFOG optical path are mainly accomplished by hand. Lots of human experience-related quality problem, such as the scratch or the abrading of fiber surface, and the adhesive dispensing operation, may happen which will influence the final assembly quality.

The defect-caused optical path energy leakage is a rare-happened but intolerant quality problem when assembling IFOG optical path. It indicates the breakage and the energy loss of the assembled fibers. The defect may be caused by the abrasion of fiber surface or the overstepping of the maximum bend radius [6]. When the assembly task is implemented by an inexperienced engineer or if the IFOG works in an extreme application environment this defect may happen. In some cases, the vibration and the impulsion may also cause the inner layout change of IFOG optical path. Thus the improper assembly layout and the material aging may induce defect. Currently, the research and report of defect-caused energy leakage issue are rare because the designer never meets that problem while the manufacturing engineer does not have effective tools to detect it. This problem decreases the quality and the reliability of IFOG product.

In this paper, the non-destructive testing and the assembly quality evaluation techniques of IFOG optical path are proposed. Considering of the different assembly orders, such as the open or the close loop states of different optical path components, the optical path is divided into three parts: the front-end optical path, the back-end optical path, and the inner side of fiber optic coil. The front-end optical path includes the light source, the detector, and the coupler. The back-end optical path refers to the integrated optical chip. And the inner side of fiber optic coil indicates the winded parts of the fiber optic coil. Three non-destructive testing methods are developed: the laser injection method, the Optical Time Domain Reflectometer (OTDR) method [7], and the infrared image analysis method [8]. The corresponding tools and models are developed to collect and analyze the defect data. Finally, the Support Vector Machine (SVM) classifier [9] is used to evaluate the assembly quality and reliability.

In the following sections, first the IFOG optical path assembly issue will be presented. Second, the non-destructive testing methods will be addressed. Finally, some experiment results and discussions will be given.

## 2. Optical path assembly issue of IFOG

Fig. 2 (a) shows the assembly orders and the splicing states of a kind of IFOG. The numbers inside of circles represent the assembly orders. In (a), the optical path is divided into three parts by rectangles. The left rectangle is the front-end optical path. The laser injection method can be utilized to detect the defect because that part has an empty port. The middle rectangle is the back-end optical path. The infrared image analysis method can be used here because its optical path is closed. The right rectangle is the inner side of fiber optic coil. The OTDR method can be employed to analyze defect before the connection of the fiber optic coil and the integrated optical chip. The infrared image analysis method can also be used to check the assembly quality of the entire optical path. Fig. 2 (b), (c), and (d) show the typical defect cases: the large bending radius-caused defect, the abrasion-caused defect, and the large stress-caused defect.

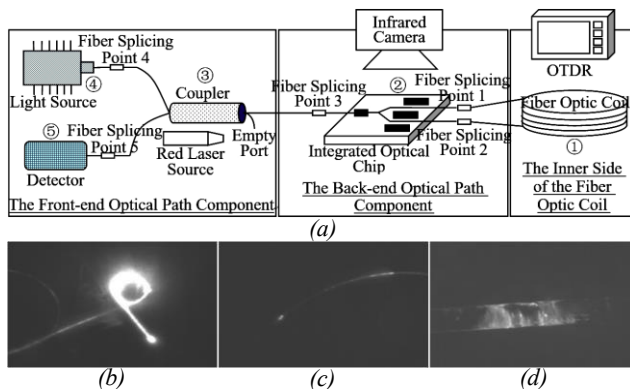


Fig. 2. The assembly sketch map of a kind of IFOG and its defect samples

Table 1 shows the typical defect types and their explanations of the IFOG optical path assembly. In general, a fiber includes [10] the core, the cladding, and the coating. From Table 1, the defect issues can be classified into three types. The first type is the fiber quality-caused defect: both the cladding and the coating have distinctive defects because the mechanical abrading or the stress crack happens. The second type is also a kind of fiber defect-caused problem: only the coating has distinctive defects in that situation because of the improper splicing or the stress influence. The cladding is unbroken in that case. The third type is the improper assembly-caused defect: only the coating has mini defects because the small bending radius or the glue-caused materials degeneration happens. Regarding a practical application, only the third type of defect is tolerable from the product manufacturing point of view.

Table 1. The defect types and their explanations

| No. | Defect phenomenon                                   | Defect explanation  | Defect type     |
|-----|---|---|-----------------|
| 1   | Both cladding and coating have distinctive defects. | Mechanical abrading, fiber break off, or stress destroy, etc.                     | Fiber defect    |
| 2   | Only coating has distinctive defects.               | Fiber splicing, stress destroy, etc.  | Fiber defect    |
| 3   | Only coating has mini defects.                      | Small bending radius, glue-caused material degeneration, or stress extrusion etc. | Assembly defect |

## 3. Defect detection methods

### 3.1. The laser injection method

The laser injection method uses the high power red laser device to test the turnoff state of an optoelectronic element. It injects rays into element from one open end and observes the output from the other open end. Fig. 3 shows the principle chart of this method. In Fig. 3, (a) is a standard sketch map of that method. The red laser device casts rays into an optic lens. The rays are converged and injected into one open end of fiber. Then a light receiver gathers the output rays from the other open end of fiber. Finally the turnoff state of fiber can be evaluated by the comparison of light energy attenuation [11]. Image (b) is the sketch map of our proposed method: a visible light camera is used to observe the surface of fiber; then the defect detection can be carried out by computing the average intensity of image pixels in the broken region.

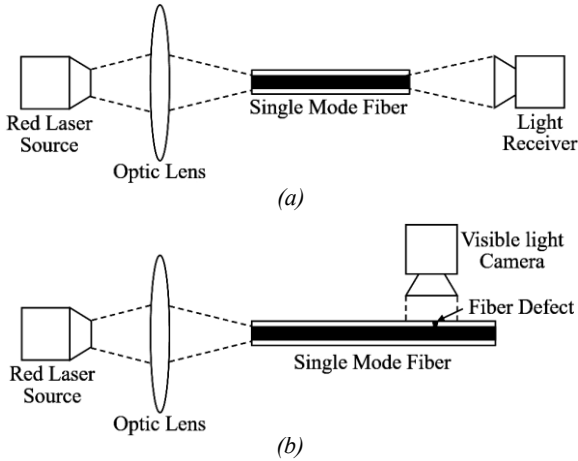


Fig. 3. The principle charts of laser injection method

### 3.2. The OTDR method

The OTDR is a standard optical path analysis device. It can measure the energy distribution of light signal and identify the abnormal light attenuation. When it works, the light pulse is injected into one fiber end; then the Rayleigh backscattering light and the Fresnel reflection light [12] can be observed by a detector; finally the abnormal regions and their energy losses can be estimated. Fig. 4 shows the sketch map of an OTDR output curve. From Fig. 4 four-type of abnormalities can create significant influence in that curve. For example, the fiber splicing region may decrease the output intensity; the fiber connector will create energy loss; and the impurities inside of fiber, such as the material particles or the air particles, will induce changes. And the defect of fiber can also make abnormalities. The output of OTDR will become a noise series if the turnoff happens. The merit of OTDR method is obvious; however its shortcoming is also evident: it can only be used to measure the working state of an open loop optical path.

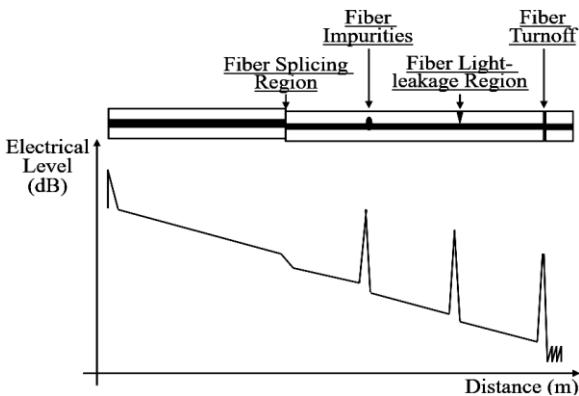


Fig. 4. The abnormality samples of OTDR output data

### 3.3. The infrared image analysis method

The infrared image analysis method utilizes the infrared camera to observe the defect of fiber surface. The measurement ranges of infrared camera can be from 900nm to 1700nm. Because the size of IFOG optical path is small, a five Degree Of Freedom (DOF) movement control platform is developed to realize the attitude tuning. The vertical motion, the horizontal motion, the rotation motion, and the 30° angle motion, are all supported by that platform. Fig. 5 (a) shows the structure of that system. An image analysis method is utilized to detect and segment the defect region. Fig. 5 (b) is the computational flow chart of that method. From Fig. 5 (b), after the image preprocessing, such as the enhancement and the definition check, the region segmentation technique [15] is employed to detect and mark the defect pixels; then the image features [14] of defect region can be computed. Finally the defect type can be deduced.

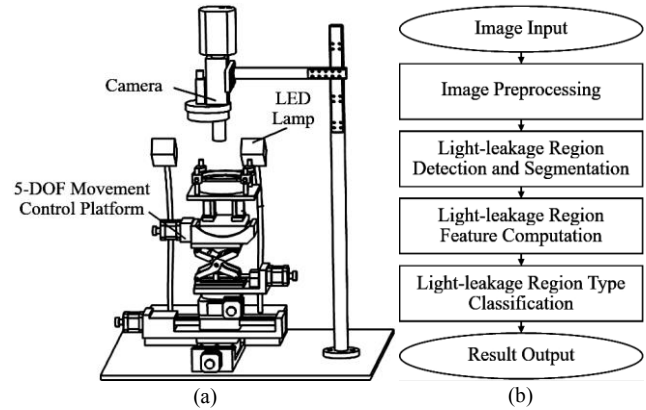


Fig. 5. The corresponding device and the computation flow chart of infrared image analysis method

Many image segmentation methods can be employed to label the image defect regions. Considering of the computational precision, both the flood fill algorithm and the graph cut model can be used [2]. The flood fill algorithm is a traditional image segmentation method which can mark the defect pixels by the principle of threshold-based merging. The segmentation principle of flood fill method is shown by (1). The graph cut method is a new developed tool which can segment the defect pixels by using the principle of graph theory [13]. Its energy function design method [14] is presented by (2). Regarding the defect segmentation task of defect region, if the image definition is high, the graph cut method can be utilized; otherwise the flood fill method should be employed. These segmentation techniques above can also be used for the image processing of visible light camera presented in section 3.1.

$$I(x_{seed}, y_{seed}) - T_1 \leq I(x, y) \leq I(x_{seed}, y_{seed}) + T_2 \quad (1)$$

$$E(A) = \lambda_1 \sum_{i \in I} E1(x_i) + \lambda_2 \sum_{(i,j) \in N, x_i \neq x_j} E2(x_i, x_j) \quad (2)$$

where  $(x_{seed}, y_{seed})$  is the coordinate of seed point;  $I(x, y)$  is the image intensity in coordinate  $(x, y)$ ;  $T_1$  and  $T_2$  are the lower and the upper thresholds;  $E1$  and  $E2$  are the energy functions,  $E1$  is the data dependent item,  $E2$  is the smoothness item;  $\lambda_1$  and  $\lambda_2$  are the weights of energy functions, and  $\lambda_1 + \lambda_2 = 1$ .

After the segmentation processing of defect regions, the energy leakage intensity of them can be estimated. Here the energy leakage intensity is only a kind of image feature, not a standard physical quantity. In (3), according to Planck's blackbody spectral radiation law [15], the spectral emitting function of blackbody is related with the wavelength and the temperature. Regarding other bodies, the computation of spectral emitting function is also related with the materials character [16]. In (3), the radiant emittance function  $\varepsilon_\lambda(T)$  is an uncertain variable, i.e. it should be calibrated and measured by some special experiments and devices. In this paper, the radiant emittance function  $\varepsilon_\lambda(T)$ , whose distribution scope is 0.7~0.9 (the application temperature is from 0°C to 100°C), is used to assess the intensity leakage of fiber. When estimating the intensity leakage, the equations (4), (5), and (6) are used to assess the defect intensity from the infrared image. Because the edge pixels of the segmentation result are always not accurate, a punishment weight  $\omega_2$  is used to decrease the estimation error.

$$M_\lambda(T) = \varepsilon_\lambda(T) \cdot M_{0\lambda}(T) = \varepsilon_\lambda(T) \cdot \frac{c_1}{\lambda^5} \frac{1}{\exp(c_2/\lambda T) - 1} \quad (3)$$

$$E_k \approx \sum_{(i,j) \in R} w(i,j) I(i,j) \varepsilon_{\lambda_k}(T) \frac{c_1}{\lambda_k^5} \frac{1}{\exp[c_2/\lambda_k T] - 1} \quad (4)$$

$$w(i,j) = \begin{cases} \omega_1 & \text{if } (i,j) \notin \text{edge} \\ \omega_2 & \text{else} \end{cases} \quad (5)$$

$$E = \sum_{k \in \{\lambda_1, \lambda_2, \dots\}} E_k \quad (6)$$

where  $\varepsilon_\lambda(T)$  is a radiant emittance function at temperature  $T$ ;  $M_{0\lambda}(T)$  is a spectral emitting function of blackbody at temperature  $T$ ,  $c_1 = 3.741832 \times 10^{-16}$  W·m<sup>2</sup>,  $c_2 = 0.01438786$  m·K;  $\lambda$  is the wavelength;  $\lambda_k$  is the  $k^{\text{th}}$  wavelength;  $I(i, j)$  means the pixel intensity in position  $(i, j)$ ;  $(i, j) \in R$  means the pixel in position  $(i, j)$  belongs to defect region  $R$ ;  $w(i, j)$  is a weight,  $\omega_1, \omega_2 \in (0, 1]$ .

#### 4. Reliability analysis of optical path assembly

The final target of defect analysis is to control the assembly quality of IFOG optical path. Traditionally, the physical prototype-based model and the probability or statistics-based method can be used. The physical prototype-based model uses the physical hypothesis [17] to describe the change laws of objective phenomenon; while the probability or statistics-based model uses the life distribution or the failure probability [18] to analyze the reliability of complex system. The data-driven-based model is a new developed method. It uses the machine learning theory [19] to assess the quality of complex product. It does not have severe application requests on sample data. Regarding the defect analysis issue, the data-driven-based model is used here for two reasons: first, because of the comparable small manufacturing requirement, the accumulated data of IFOG optical path are still small currently; thus the probability or statistics models cannot be used without enough data support. Second, no proper optical path assembly simulation model can be used for this problem; thus the physical model-based method also cannot be considered.

The SVM is used to build the reliability analysis model of optical path assembly. In this paper the product quality degree is just classified into qualified and unqualified. The design of SVM considers a ten-input one-output classifier. Fig. 6 shows the reliability evaluation sketch map of optical path assembly. The training data of SVM can be written by  $T = [a_0, a_1, a_2, a_3, a_4, a_5, a_6, a_7, a_8, a_9, a_{10}]$ ; where  $a_0$  is the defect intensity of fiber between light source and coupler;  $a_1$  is the defect intensity of fiber between detector and coupler;  $a_2, a_3, a_4, a_5, a_6$  are the defect intensities of five splicing points;  $a_7$  is the number of defect point in fiber optic coil;  $a_8$  is the intensity loss of fiber optic coil;  $a_9$  is the intensity loss of abrading caused defect;  $a_{10}$  is the intensity loss of the small bending radius-caused defect. The parameters  $a_0$  and  $a_1$  are measured by the laser injection method;  $a_2, a_3, a_4, a_5, a_6, a_9$ , and  $a_{10}$  are estimated by the infrared image method; and  $a_7, a_8$  are measured by the OTDR method. The supervising data of SVM is the IFOG bias stability [20]. The C-SVC [21] is utilized here because of its stability. Equations (7) and (8) are the criterion and the kernel functions of it.

$$f(x) = \text{sgn} \left\{ \sum_{i=1}^n \alpha_i^* y_i K(x_i, x) + b^* \right\} \quad (7)$$

$$K(x, z) = \exp \left[ -\frac{\|x - z\|^2}{\sigma^2} \right] \quad (8)$$

where  $\alpha_i^*$  is the Lagrange multipliers;  $b^*$  is the threshold of classification function;  $\text{sgn}(\cdot)$  is the sign function;  $\sigma$  is the control parameter of a radial basis kernel function  $K(x, z)$ .

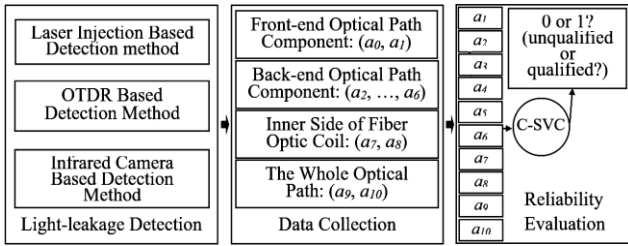


Fig. 6. The reliability evaluation flow chart of IFOG optical path assembly

### 5. Experiments and discussions

Many experiments are implemented to test the validity of proposed techniques and methods. The optical path components of a kind of IFOG participate the test experiments. An image analysis and IFOG assembly quality evaluation software is developed in our PC (Intel(R) Core (TM) i5-3337U CPU, 1.8GHz, 4.0GB RAM) by C coding. The infrared image collection experiments are carried out in a dark room.

#### 5.1. Application and evaluation of laser injection method

Fig. 7 shows the apparatus and the application cases of the laser injection method: (a) shows a fiber adapter and a red laser pen; (b) is the photo of a fiber optical path detector without any defects; (c) presents a detector with one defect point (the red pixels inside of a yellow circle mark the defect region); (d) is the image captured by a visible light camera. In this paper, the center wavelength of red laser pen can be chosen as 635nm, 650nm, or 670nm; their light power should be large than 10mW. The maximum test distance of laser injection method can reach 3.0km. After an experimental test, the laser pen with 650nm wavelength can get the best performance for our IFOG product. When using this method to detect defect, the red laser pen will inject laser into the empty port of IFOG front-end optical path; the defect can be observed by the bare eyes firstly. Then the visible light camera can be used to record and estimate the defect intensity.

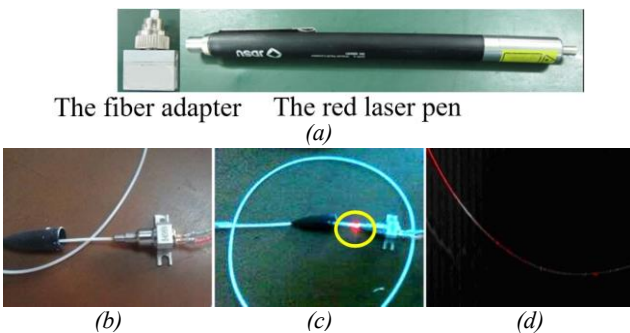


Fig. 7. The illustrations of the red laser pen, the fiber adapter, and the defect cases captured by a visible light camera

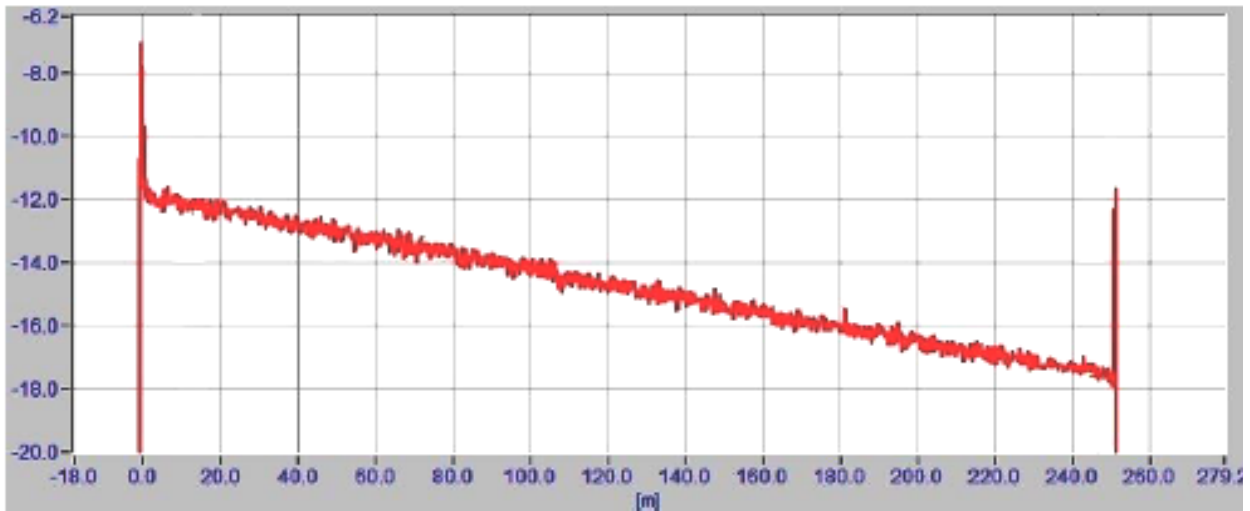
Table 2 shows the defect intensity estimation results of the laser injection method. The defect location, the defect intensity, and the defect cause are all addressed in that table. The average gray intensity of the defect region can be regarded as an evaluation index. The mark and the segmentation of defect region can be accomplished by hand. From Table 2 it can be seen that any unregulated operations may lead to micro defect in fiber surface; and the red laser injection method can make an objective and measurable record of that issue for the optical path assembly. When using the red laser pen in practice, the output end of red laser pen should be cleaned by the anhydrous alcohol before it is used; the small bending radius-caused defect should be identified and avoided; and the visible light camera can be employed to record the defect only after the light source of laser pen has reached a stable state.

Table 2. Defect intensity estimation results of front-end optical path using the red laser injection method

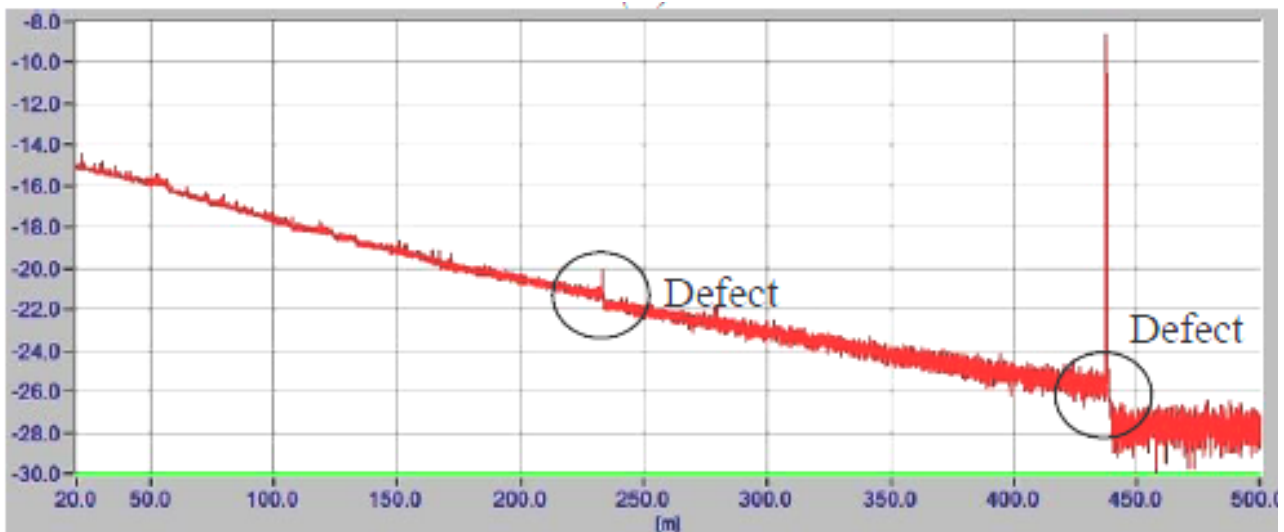
| No. | Defect location                                | Defect intensity | Defect cause        |
|-----|--|------------------|---------------------|
| 1   | Left end of fiber splicing point 4             | 38.2             | Fiber splicing      |
| 2   | Left end of fiber splicing point 4             | 121.5            | Mechanical abrading |
| 3   | Right end of fiber splicing point 5            | 48.1             | Mechanical abrading |
| 4   | Right end of fiber splicing point 5            | 78.4             | Fiber splicing      |
| 5   | Middle region between light source and coupler | 148.2            | Stress crack        |

#### 5.2. Application and evaluation of OTDR method

A kind of OTDR is utilized to detect and identify the defect of fiber optic coil. Fig. 8 shows the output curve samples of OTDR device. Image (a) shows the normal output curve. If no defect event happens, no big burr appears in that curve. Image (b) is the output with light energy attenuation. In (b), two defects appear in that curve. The defect will lead to a holistic downward movement of OTDR curve. The first defect is caused by the light transmission of fiber adapter. It can bring energy attenuation with 0.1dB to 0.5dB for the single mode fiber. The second defect is caused by the fiber turnoff. Regarding the IFOG, the acceptable total energy attenuation of fiber optic coil should be smaller than 3.0dB to 4.0dB; otherwise a quality problem should be reported.



(a)



(b)

Fig. 8. The output result samples of OTDR

Table 3 shows the OTDR measurement results of IFOG optical paths. In Table 3, the measurement results of the former three rows belong to the same fiber optic coil; while the results of the latter two rows come from another fiber optic coil. From Table 3, regarding the first coil, their individual energy attenuations are 3.9dB, 0.9dB, and 1.1dB respectively. Thus the total energy attenuation is  $3.9+0.9+1.1=5.9$ dB. Because its total energy attenuation is larger than 4.0dB, the manufacturing quality of this coil is unqualified. Differently, regarding the second coil, its total energy attenuation is only 2.5dB ( $<4.0$ dB); hence its product quality is qualified. However, even the product quality of fiber optic coil is qualified, after the assembly, the final output precision of IFOG still cannot fulfil the user's request in many cases. In these situations, the influences of micro-defect cannot be observed by the laser injection method or the OTDR method conveniently. Therefore a new analysis technique should be developed.

Table 3. Defect analysis results of the inner side of fiber optic coil using OTDR method

| No. | Defect location (m) | Fiber attenuation loss (dB) | Total length of fiber (m) |
|-----|---------------------|-----------------------------|---------------------------|
| 1   | 18                  | 3.9                         | 1250                      |
| 2   | 73                  | 0.9                         | 1250                      |
| 3   | 329                 | 1.1                         | 1250                      |
| 4   | 275                 | 1.3                         | 1800                      |
| 5   | 1018                | 1.2                         | 1800                      |

### 5.3. Application and evaluation of infrared image analysis method

Fig. 9 shows the original image samples and their processing results of infrared image analysis method. In

Fig. 9, (a), (b), and (c) are the original infrared images; (d), (e), and (f) are the corresponding segmentation results, respectively. In Fig. 9, it can be noticed the imaging diameter of (a) is smaller than the imaging diameters of (b) and (c). Therefore it is necessary to tune the capture distance and the focal distance of infrared camera so that the region segmentation results of different fibers have comparability. Currently, the judgment of fiber imaging diameter is controlled manually: the imaging diameter of single mode fiber should be 50 pixels to 55 pixels; while the imaging diameter of polarization maintaining fiber should be 30 pixels to 35 pixels. From Fig. 9 because the imaging diameter of (a) is small, its analysis result should be abandoned.

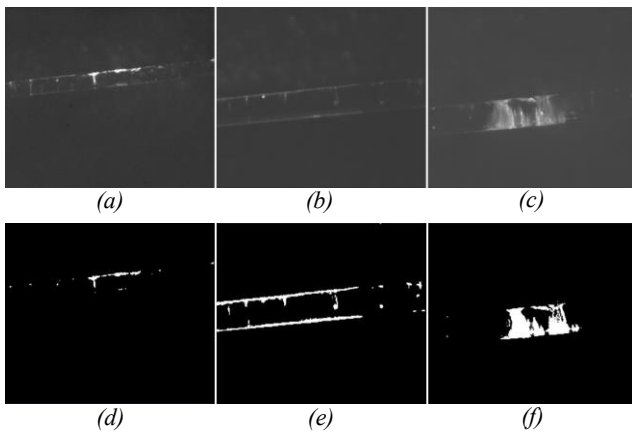


Fig. 9. The infrared image samples and their segmentation results

Table 4 shows the computation results of defect intensity estimation. According to equation (4), the final defect intensity is relative with the defect size, the light wavelength, the temperature, and the radiant emittance function. The defect size can be calculated by the image segmentation technique; the injected light wavelength also can be set or measured accurately; and the working temperature of fiber can be estimated by the environment temperature approximately. For example, if the relative humidity is 32%RH, the environment temperature can be controlled to 25°C (298.15K) in the dark room; thus the working temperature of fiber can be regarded as 298.15K. Finally, regarding the emittance function  $\varepsilon_\lambda(T)$ , its value can be set from 0.7 to 0.9 for the single mode fiber in this paper. The specific value of  $\varepsilon_\lambda(T)$  should be related with different product brands and their performances. In Table 4, the average intensity means the average gray value of all the pixels inside of defect region. The weight function  $w(i, j)$  can be set by  $\omega_1=1.0$  and  $\omega_2=0.6$ , respectively.

Table 4. Defect intensity estimation results of back-end optical path using infrared image analysis method

| Image name | Defect size | Average intensity | Radiant emittance function | Wavelength ( $\mu\text{m}$ ) | Estimated intensity           |
|------------|-------------|-------------------|----------------------------|------------------------------|-------------------------------|
| (a)        | 1850        | 108.0             | 0.83                       | 1.2                          | $\approx 5.76 \times 10^{-9}$ |
| (b)        | 2564        | 143.0             | 0.83                       | 1.2                          | $\approx 14.0 \times 10^{-9}$ |

Obviously, the intensity estimation results in Table 4 are not as accurate as the infrared image analysis result of some standard infrared radiation measurement devices [22]. The parameters setting of equation (4) is also related with the practical application experiences of different fiber types. However, the pattern recognition classifier is used here to evaluate the assembly quality of IFOG optical path. The estimated intensity in Table 4 is only a kind of feature for the classifier [23]. Thus, if the selected feature can represent the essential attribute of a physical phenomenon to some extent, this intensity computation result is meaningful for the classifier. In addition, because the size of IFOG is small, and the infrared image can be gotten conveniently by the infrared camera, this proposed method can be popularized for other practical engineering application in future.

#### 5.4. Defect analysis of optical path assembly

The C-SVC is employed to carry out the assembly quality evaluation task. After a series of performance tests, its average classification precision for our test data is about 92% when the total training data amount is 230. The LIBSVM [24] is used to realize that simulation. In Fig. 6, the input vector of C-SVC is  $T=[a_0, a_1, a_2, a_3, a_4, a_5, a_6, a_7, a_8, a_9, a_{10}]$ ; its binary output is the quality degree of IFOG bias stability. After all these elements of  $T$  are normalized into [0.0, 1.0], the vector  $T$  can be sent to classifier for the quality degree forecasting. If the organization of training data is proper, the forecast performance of C-SVC will be good. For example, the measurement data are:  $a_0=43.7$ ,  $a_1=90.7$ ;  $a_2=1.6 \times 10^{-9}$ ,  $a_3=0.8 \times 10^{-9}$ ,  $a_4=3.7 \times 10^{-9}$ ,  $a_5=4.1 \times 10^{-9}$ ,  $a_6=1.3 \times 10^{-9}$ ,  $a_7=7.2 \times 10^{-9}$ ,  $a_8=5.7 \times 10^{-9}$ ;  $a_9=2.0$ ,  $a_{10}=2.1$ ; after the practical computation, the forecasted bias stability is unqualified. Table 5 shows the comparisons of IFOG bias stability between the computed result and the measured result. From Table 5 it can be seen the proposed method can realize the assembly quality evaluation well. And with the accumulation of training data, the estimation precision of C-SVC can be improved in future definitely.

Table 5. The IFOG bias stability comparisons between the measured result and the computed result

| No. | The measurement result of bias stability | The estimation result of bias stability <sup>a</sup> |
|-----|--|--|
| 1   | 1.01°/h (qualified)                      | qualified  |
| 2   | 0.74°/h (qualified)                      | qualified  |
| 3   | 1.91°/h (unqualified)                    | unqualified  |

<sup>a</sup> The bias stabilities of qualified product and unqualified product are [0.34, 1.56] and [1.56, 2.78] respectively according to the practical assembly experiences.

To assess the proposed technique further, the first time pass rate of IFOG product is investigated here. Here the first time pass rate means the product which can pass the quality check once it is manufactured without any reworks. Fig. 10 shows the first time pass rate comparisons before and after the application of proposed techniques. The left

blue columns are the results before the application of proposed techniques; the right red columns are the results after the application of proposed techniques. In Fig. 10, the different IFOG products and the same IFOG product manufactured in different batches are compared. Fig. 10 (a) is the first time pass rate comparisons of different IFOG products. Product A and product B are some kinds of low precision products; while product C belongs to the middle precision product. Fig. 10 (b) shows the first time pass rate comparison of the same IFOG manufactured in different batches. From Fig. 10, it can be seen that the proposed non-destructive detection method and quality evaluation technique can improve the final product quality degree to some extent.

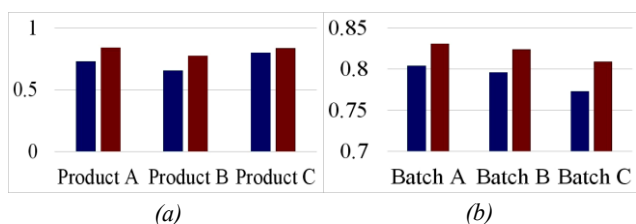


Fig. 10. The first time pass rate comparisons of IFOG optical path assembly before and after the application of proposed techniques

### 5.5. Discussions

The IFOG is a kind of all-solid-state and mini-type sensing device in the inertial navigation product family. Because of its high precision but small size, light weight and low power consumption, the application of it is convenient and wide in recent years. However, one of its problems is that its optoelectronic parts and components of optical path are easy to be damaged during the manufacturing and the assembly procedures. Many minor defects which cannot be clearly observed by engineer may happen. They include the low quality component selection, the improper layout, or the human error-caused assembly problem, etc. Currently, no enough nation or enterprise standards are made to restrict its manufacturing and assembly processes; and no effective methods can be used for quality monitor purposes. This is because on one hand the size of IFOG product is very small; and on the other hand the current parameters, the voltage parameters, or some other optical parameters cannot be measured easily from it.

In this paper, the non-destructive testing technique is developed to detect the fault when assembling the IFOG optical path. This technique not only involves the testing of the entire parts of IFOG optical path but also covers the total stages during the manufacturing and assembly courses. The red laser pen, the OTDR device, and the infrared camera, etc. are all utilized. A kind of image analysis method is also designed to analyze the assembly components. After the testing of IFOG optical path, the SVM classifier is considered to evaluate the assembly quality. It is well known that the classifier is a kind of tool

which can realize the analysis and the forecasting of complex or abstract dataset. The SVM is still effective when the size of training data is small. In final, by the use of testing data captured during the manufacturing and assembly procedures and the SVM classifier, the assembly quality of optical path can be evaluated and controlled objectively.

### 6. Conclusion

A series of non-destructive testing and assembly quality evaluation methods for the optical path assembly of a kind of IFOG are presented. First, the optical path of IFOG is divided into three parts according to their assembly orders. The front-end optical path, the back-end optical path, and the inner side of fiber optic coil, are defined. Second, the laser injection method, the OTDR-based method, and the infrared image analysis-based method, are considered to detect the defect of IFOG optical path. Finally, the SVM classifier is utilized to evaluate the quality and the reliability. In future, more test data will be accumulated for the classifier training, and some elaborated image analysis methods will be developed.

### Acknowledgments

This work is supported by the National Natural Science Foundation of China under grant No. 61501016 and the Fundamental Research Fund for the China Central Universities of USTB under grant No. FRF-BD-17-002A.

### References

- [1] W. Wang, Introduction of the Interferometric Fiber Optic Gyroscope Technology, 1st ed., China Aerospace, Beijing (2010).
- [2] H. Liu, W. Wang, F. Gao, J. Li, K. Chen, Infrared Phys. Technol. **66**, 125 (2014).
- [3] J. Hao, B. Liu, Proc. ICMTMA, IEEE, Shanghai, China, 906 (2011).
- [4] X. Li, C. Zhang, Z. He, Proc. ISSCAA, IEEE, Shenzhen, China, 1, (2008).
- [5] M. Pamela, Ergonomics: Foundational Principles, Applications, and Technologies, Taylor & Francis (2011).
- [6] R. M. Kingsta, A. Sivanantharaja, Proc. ICICES, IEEE, Chennai, India, 769 (2013).
- [7] D. V. Caballero, J. P. Von Der Weid, P. J. Urban, Proc. SBMO/IEEE MTT-S IMOC, IEEE, Rio de Janeiro, Brazil, 1 (2013).
- [8] W. Zhang, Y. Song, Z. Yang, M. Li, G. Tian, Proc. SPIE **7659**, 76590V-1 (2010).
- [9] B. Liu, D. Hou, P. Huang, B. Liu, H. Tang, W. Zhang, P. Chen, G. Zhang, Nondestruct. Test Eva. **28**(4), 367 (2013).

- [10] C. Decusatis, Handbook of Fiber Optic Data Communication, 4th ed., Academic 2013.
- [11] N. Amitay, H. M. Presby, F. V. Dimarcello, J. Lightwave Technol. **5**(1), 70 (1987).
- [12] S.-C. Lin, S.-L. Lee, H.-H. Lin, G. Keiser, R. J. Ram, J. Lightw. Technol. **29**(24), 3727 (2011).
- [13] H. Liu, W. Wang, X. Li, F. Li, Proc. IEEE ROBIO, IEEE, Guangzhou, 1968 (China).
- [14] H. Liu, W. Wang, L. Shi, Infrared Laser Eng. **41**(11), 3123 (2012).
- [15] J. Wang, L. Xu, F. Wang, Proc. SPIE **8002**, 80020C-1 (2011).
- [16] J. Cipar, G. Anderson, and T. Cooley, Proc. MIPPR, IEEE, Lisbon, Portugal, 1, (2011).
- [17] K. Lakshmi, A. R. M. Rao, Nondestruct. Test Eva. **29**(4), 357 (2014).
- [18] X.-S. Si, W. Wang, C.-H. Hu, D.-H. Zhou, M. G. Pecht, IEEE Trans. Rel. **61**(1), 50 (2012).
- [19] J. Wu, IEEE Trans. Knowl. Data Eng. **24**(1), 1 (2012).
- [20] O. Celikel, S. E. San, IEEE Sensors J. **9**(2), 176 (2009).
- [21] W. Zeng, J. Jia, Z. Zheng, C. Xie, L. Guo, Proc. BMEI, IEEE, Shanghai, China, 1621 (2011).
- [22] W. Guan, L. Guo, L. Fu, Proc. CCDC, IEEE, Changsha, China, 1863 (2014).
- [23] B. Ribeiro, IEEE Trans. Syst. Man. Cybern. C, Appl. Rev. **35**(3), 401 (2005).
- [24] <http://www.csie.ntu.edu.tw/~cjlin/libsvm/>

---

\*Corresponding author: imkyran@hotmail.com